

See discussions, stats, and author profiles for this publication at: <https://www.researchgate.net/publication/260432299>

Scanning Tunneling Microscopy Investigation of Ultrathin Titanium Oxide Films Grown on Pt₃Ti(111)

ARTICLE in THE JOURNAL OF PHYSICAL CHEMISTRY C · FEBRUARY 2014

Impact Factor: 4.77 · DOI: 10.1021/jp4105213

CITATIONS

2

READS

54

6 AUTHORS, INCLUDING:



Maria Buchholz

Karlsruhe Institute of Technology

15 PUBLICATIONS 66 CITATIONS

SEE PROFILE



Séverine Le Moal

Université Paris-Sud 11

15 PUBLICATIONS 62 CITATIONS

SEE PROFILE



C. Becker

Aix-Marseille Université

91 PUBLICATIONS 1,418 CITATIONS

SEE PROFILE



Klaus Rainer Wandelt

University of Bonn

436 PUBLICATIONS 8,207 CITATIONS

SEE PROFILE

Scanning Tunneling Microscopy Investigation of Ultrathin Titanium Oxide Films Grown on Pt₃Ti(111)

Christian Breinlich,[†] Maria Buchholz,^{†,‡} Marco Moors,^{*,†,§} Séverine Le Moal,^{†,||} Conrad Becker,^{†,⊥} and Klaus Wandelt^{†,‡,#}

[†]Institute of Physical and Theoretical Chemistry, University of Bonn, Wegelerstraße 12, D-53115 Bonn, Germany

[‡]Institute of Functional Interfaces, Karlsruhe Institute of Technology, D-76021 Karlsruhe, Germany

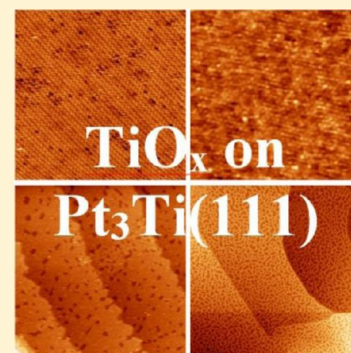
[§]Peter Grünberg Institute, Forschungszentrum Jülich, Wilhelm-Johnen-Straße, D-52425 Jülich, Germany

^{||}Institut de Chimie Moléculaire et des Matériaux d'Orsay, Université Paris Sud, UMR 8182, F-91405 Orsay Cedex, France

[⊥]Centre Interdisciplinaire de Nanoscience de Marseille, Aix-Marseille Université, UMR 7325, Campus de Luminy, Case 913, F-13288 Marseille Cedex 09, France

[#]Institute of Experimental Physics, University of Wrocław, Pl. Maksa Borna, 50-204 Wrocław, Poland

ABSTRACT: Ordered ultrathin titanium oxide films have been produced under ultrahigh vacuum (UHV) conditions by oxidation of a Pt₃Ti(111) single crystal at elevated temperatures. Depending on substrate temperature, oxygen dosage, and partial pressure, four different titania phases have been observed. All phases have been investigated by low-energy electron diffraction (LEED) and scanning tunneling microscopy (STM). Two commensurate phases with a rect-(6 × 3√3) and a hex-(7 × 7)R21.8° superstructure, respectively, are obtained at low oxygen pressures. Both structures form homogeneous films, which wet the complete surface and are stable against further annealing. At high oxygen partial pressures two incommensurate structures can be prepared. The first one contains several holes to release stress arising from the lattice mismatch between the oxide film and substrate. The second one shows a very rough surface morphology and is, like the other incommensurate phase, unstable against thermal treatment. The structures of the different phases are very similar to the structures found for the systems TiO_x/Pt(111), VO_x/Rh(111), and VO_x/Pd(111), which have been described extensively in the literature.



1. INTRODUCTION

Ultrathin films of metal oxides exhibit novel structural and electronic and, hence, physical and chemical properties compared to their bulk counterparts, which makes them interesting for many applications, e.g., in microelectronic devices and catalysis. Ultrathin films grown on a metal support have the advantage that they can be studied with nearly all spectroscopic surface science techniques, in particular those based on charged particles, which is not the case for many undoped bulk oxide surfaces like, e.g., Al₂O₃ or unreduced TiO₂ due to their low conductivity. Titanium oxides are frequently investigated for their interesting catalytic properties and are often mentioned in relation to the so-called strong metal support interaction (SMSI) effect, which opens a pathway to the tailoring of specific catalysts for different chemical reactions.

After the first studies of Boffa et al.¹ on atomically thin TiO_x films grown on Pt(111) this system was investigated in depth by Granozzi et al.^{2–6} They prepared TiO_x films by reactive evaporation of titanium on Pt(111) and subsequent annealing steps in oxygen atmosphere. Six different thin titania phases were found and characterized^{2–6} showing either commensurate or incommensurate superstructures with hexagonal or rectangular unit cells. All phases except one stoichiometric TiO₂ phase proved to be composed of a Ti–O bilayer with titanium at the

interface. For some phases a great similarity to thin vanadium oxide films was found.^{7–10}

Our approach is, in analogy to former experiments in our group on the oxidation of a Ni₃Al(111) surface,^{11–14} to use a binary Pt₃Ti(111) single crystal surface to prepare ultrathin TiO_x films at elevated temperatures. Such intermetallic alloys with a remarkably high heat of formation show a significantly reduced reactivity compared to the pure metals, which can be taken advantage of to realize the growth of atomically thin oxide films with a very high degree of surface order and reproducibility. Pt₃Ti crystallizes, like Ni₃Al, in the fcc Cu₃Au structure. The bulk truncated (111) surface exhibits a p(2 × 2) superstructure of titanium atoms.^{15–20} In a recent paper²¹ we have presented a detailed atomic emission spectroscopy (AES), low-energy electron diffraction (LEED), ultraviolet photoelectron spectroscopy (UPS), and high-resolution electron energy loss spectroscopy (HREELS) study of the surface oxidation, which disclosed great similarities to the long-range properties of the films obtained by reactive Ti evaporation on Pt(111).² In this paper we present STM measurements on the

Received: October 24, 2013

Revised: February 26, 2014

Published: February 27, 2014

atomic structure of the obtained titania phases on $\text{Pt}_3\text{Ti}(111)$ and compare them to the work of Granozzi et al.^{2–6} on $\text{TiO}_x/\text{Pt}(111)$ as well as to different vanadium oxide phases.^{7–10} Thereby, we show the similarities but, in particular, also emphasize the differences of the various titanium oxide films prepared by the two distinct approaches.

2. EXPERIMENTAL METHODS

The scanning tunneling microscopy (STM) experiments have been conducted in our home-built LT-STM, which has been described in detail elsewhere.²² The STM was run at room temperature for all experiments presented in this paper. The sample was prepared in a preparation chamber, which was equipped with a sputter gun and facilities for LEED and AES, and from which the sample could be directly transferred into the LT-STM chamber. The STM tips were electrochemically etched from 0.5 mm tungsten wire and cleaned under UHV conditions by applying voltage pulses between -10 and $+10$ V of 10 ms duration.

The $\text{Pt}_3\text{Ti}(111)$ crystal was obtained from MaTeck (Jülich, Germany) and was cleaned by several cycles of argon sputtering at 900 K for 10 min and subsequent thermal annealing at 1100 K for 10 more minutes. Cleanliness was achieved when a sharp (2×2) superstructure was visible in LEED and no carbon and oxygen contaminations were found by AES.²¹ The preparation of the oxide films was done by dosing different amounts of oxygen at partial pressures between 10^{-8} and 10^{-5} mbar and sample temperatures ranging from 800 to 1000 K. The base pressure was always in the 10^{-10} mbar range in both chambers.

3. RESULTS AND DISCUSSION

3.1. Preparation of the TiO_x Films and LEED Results.

The Pt_3Ti alloy forms an fcc Cu_3Au structure, in which the Ti atoms are situated at the corners and the Pt atoms at the face centers of the unit cell. By cutting a single crystal parallel to a (111) plane a bulk terminated surface is obtained, in which the titanium atoms form a $p(2 \times 2)$ superstructure with respect to the $\text{Pt}(111)$ lattice. The interatomic distance within the $\text{Pt}_3\text{Ti}(111)$ surface is with a value of 2.76 Å, very similar to that of $\text{Pt}(111)$, and all superstructures observed in LEED will be described in relation to the (1×1) pattern of a $\text{Pt}(111)$ surface. The result of the oxidation process strongly depends on sample temperature and oxygen dosage. Up to now we found four different oxide phases, whose LEED patterns have been analyzed in a recent paper.²¹ All four superstructures, in principle, are also accessible by reactive evaporation of titanium onto $\text{Pt}(111)$ as shown by Sedona et al.,² but with a somewhat more complex and less reproducible preparation compared to the direct oxidation of the alloy surface. While in the latter case with temperature and oxygen dosage only two parameters have to be controlled, the formation of the titania phases on $\text{Pt}(111)$ also depends strongly on the rate and final amount of titanium deposition. Furthermore, due to its lower reactivity the use of the $\text{Pt}_3\text{Ti}(111)$ surface has the advantage of a more controlled oxidation process, which in the end results in a better film growth.²¹ Figure 1 summarizes the LEED results of the four different phases. The designation of the different phases was introduced by Sedona et al.² and is adopted here to facilitate comparison. It refers to the appearance of the individual phases in STM, namely, z = zigzag-like and w = wagon-wheel-like.

At a sample temperature of 1000 K and depending on the used oxygen dose two commensurate phases with large unit

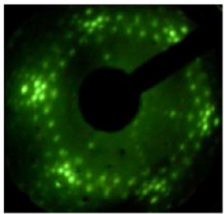
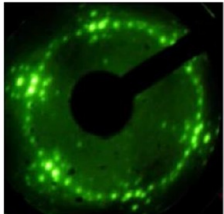
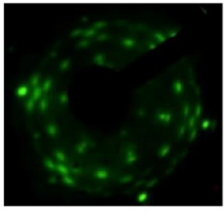
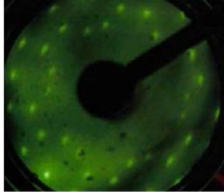
| | | |
|---|---|---|
|  | z' - TiO_x -phase $\begin{bmatrix} 6 & 0 \\ 3 & 6 \end{bmatrix}$ commensurate $(6 \times 3\sqrt{3})$ 16.6×14.4 Å rect. | $T = 1000$ K 10 - 200 L O_2 $p = 4 \cdot 10^{-8}$ mbar |
|  | w' - TiO_x -phase $\begin{bmatrix} 8 & 3 \\ -3 & 5 \end{bmatrix}$ commensurate $(7 \times 7)R21.8^\circ$ 19.3×19.3 Å hex. | $T = 1000$ K 220 - 4500 L O_2 $p = 4 \cdot 10^{-7}$ mbar |
|  | z - TiO_x -phase $\begin{bmatrix} 2.5 & 0 \\ 1.8 & 3.6 \end{bmatrix}$ incommensurate 6.8×8.6 Å rect. | $T = 800$ K 900 L O_2 $p = 3 \cdot 10^{-5}$ mbar |
|  | rect- TiO_2 -phase $\begin{bmatrix} 1.16 & 0.28 \\ 0.58 & 1.56 \end{bmatrix}$ incommensurate 3.8×3.0 Å rect. | $T = 800$ K 4500 L O_2 $p = 3 \cdot 10^{-5}$ mbar |

Figure 1. Summary of the different LEED-derived titanium oxide phases found on $\text{Pt}_3\text{Ti}(111)$. All LEED patterns were conducted with an energy of 73 eV. (a) The z' -phase is derived by oxidation of the $\text{Pt}_3\text{Ti}(111)$ crystal with a dosage between 10 and 200 L of O_2 at 1000 K. (b) Oxidation of the crystal with oxygen dosages of 220–4500 L at 1000 K results in the w' -phase. (c) The z -phase is obtained by oxidation with 900 L of O_2 at 900 K. (d) The incommensurate rect- TiO_2 phase is formed at 900 K and high oxygen dosages of 4500 L.

cells are accessible on the $\text{Pt}_3\text{Ti}(111)$ surface. For doses smaller than 200 L and a partial pressure in the 10^{-8} mbar range, the z' -phase with a rectangular $(6 \times 3\sqrt{3})$ superstructure is obtained. This phase is stable during further annealing at high temperatures. For oxygen amounts larger than 200 L a hexagonal commensurate phase with a $(7 \times 7)R21.8^\circ$ superstructure is obtained, which is also stable during further annealing.

The application of higher oxygen doses leads to two incommensurate phases with small rectangular unit cells. Oxidation at 900 K with 900 L of oxygen (at 10^{-5} mbar) yields the z -phase with a rectangular unit cell of 6.8 Å \times 8.6 Å. This phase proved to be only metastable, as it undergoes a phase transition toward the w' -phase upon further annealing at temperatures above 900 K. An initial oxidation temperature higher than 900 K usually leads directly to the w' -structure.

The rect- TiO_2 phase is obtained with very high amounts of oxygen of at least 4500 L (exposed at 10^{-5} mbar) and a surface temperature of 800 K. It possesses a rectangular unit cell of 3.0 Å \times 3.8 Å and is also metastable, as it undergoes also a phase transition toward the w' -phase upon further annealing at temperatures above 900 K. The w' -phase is also directly formed if the initial oxidation temperature is higher than 900 K. The

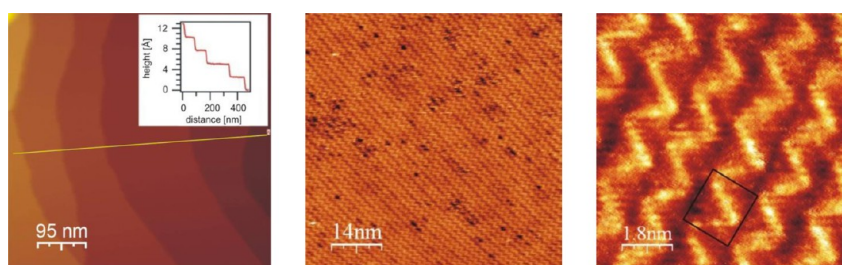


Figure 2. STM images of the rect-($6 \times 3\sqrt{3}$)-phase (z' -phase): (a) $500 \times 500 \text{ nm}^2$, $U_B = 1 \text{ V}$, $I = 60 \text{ pA}$. The inset shows a distribution of 2.3 \AA high steps in the z' -phase; (b) $70 \times 70 \text{ nm}^2$, $U_B = 0.91 \text{ V}$, $I = 50 \text{ pA}$; (c) $10 \times 10 \text{ nm}^2$, $U_B = 850 \text{ mV}$, $I = 60 \text{ pA}$.

formation of both the z - and the rect- TiO_2 phase requires high oxygen partial pressures. The same doses at low pressure (10^{-8} mbar) always lead to the formation of the w' -phase.

3.2. z' -Phase. According to the LEED measurements the rect-($6 \times 3\sqrt{3}$) phase has a rectangular unit cell of $16.6 \text{ \AA} \times 14.4 \text{ \AA}$ size. In the Matrix notation the structure can be expressed by

$$\begin{bmatrix} 6 & 0 \\ 3 & 6 \end{bmatrix}$$

Figure 2 shows STM images of this phase measured at different scales. The overview image (Figure 2a) shows a very flat and homogeneous film that covers the whole surface. Line scans across the terraces reveal typical step heights of single layers of Pt_3Ti ($\sim 2.3 \text{ \AA}$), indicating a homogeneous thickness of the film on all terraces (see inset of Figure 2a). As the film is completely closed it is not possible to determine its thickness from STM images. The film consists of stripes exhibiting a zigzag motif (Figure 2b and c), which are separated by small trenches. According to both LEED and STM images three rotational domains exist, which are induced by the $p3m$ symmetry of the substrate. The stripes are 1.4 nm wide, and the trenches between them are separated by 1.8 nm . However, not all trenches have the same depth; deeper and more shallow trenches alternate. In Figure 2b also some defects are visible, which all appear as black holes and are situated within the trenches between the stripes. The high-resolution image (Figure 2c) shows how the rectangular unit cell observed by LEED can be constructed around one elbow of the zigzag motif. Though the image is not completely resolved atomically, it seems that each zigzag-line consists of five bright protrusions.

The appearance of this phase, both in LEED and STM images, is almost identical with the z' -phase observed by Granozzi et al. on $\text{Pt}(111)$ after reactive deposition of titanium and subsequent annealing at 637 K .^{2,6} The only observable difference is that the bendings of the zigzag lines in our image always exhibit a V-shape, whereas on $\text{Pt}(111)$ sometimes alternating sequences of V- and W-shaped kinks are visible (see Figure 3). On the basis of these data a structural model of the phase was proposed and compared to DFT calculations from

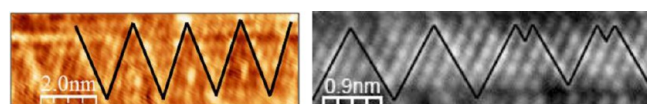


Figure 3. STM images of the z' -phase: (a) on $\text{Pt}_3\text{Ti}(111)$ ($10.0 \times 4.0 \text{ nm}^2$, $U_B = 0.97 \text{ V}$, $I = 50 \text{ pA}$) and (b) the corresponding z' - TiO_x phase on $\text{Pt}(111)$ ($6.0 \times 3.2 \text{ nm}^2$, $U_B = 0.8 \text{ V}$, $I = 1.5 \text{ nA}$) reproduced from Sedona et al.²

Barcaro et al.⁴ According to XPS the z' -phase consists of a Ti–O bilayer with the titanium atoms situated at the interface.^{2,6} This is in agreement with former measured HREELS data, which show a single loss peak at 525 cm^{-1} .²¹ This peak is characteristic for a system with Ti–O stoichiometry. The DFT calculations predict a $\text{TiO}_{1.25}$ stoichiometry and suggest the following structure model:²³ As the lattice constant for hexagonal titania ranges from 2.9 to 3.3 \AA , a strong lattice mismatch with the substrate (2.76 \AA) arises. Consequently, the titanium layer forms regions of densely packed titanium atoms (the stripes) and less densely packed regions (the troughs). The terminating oxygen layer solves the misfit problem by the formation of dislocation lines resulting in two different kinds of titanium atoms: 4-fold oxygen-coordinated titanium atoms, which form the zigzag lines, and 3-fold coordinated titanium atoms in the other regions. With positive bias voltages the empty metal states of the titanium are imaged. Due to their different electronic environment (the 4-fold coordinated titanium atoms possess formally a higher oxidation state) the atoms within the zigzag line are imaged brighter. This model is actually a refined version from a model proposed by Jennison et al.²⁴ for encapsulated Pt clusters on $\text{TiO}_2(110)$. STM images from these clusters show also a striped pattern with a zigzag motif and a rectangular, slightly distorted unit cell with the approximate size of $13.85 \text{ \AA} \times 16.85 \text{ \AA}$. Obviously, no LEED data are available from the encapsulated Pt clusters to specify the exact symmetry and size of the unit cell more precisely.²⁴ However, the proposed model also consists of a Ti–O bilayer on a hexagonal Pt layer, in which the titanium atoms are again situated at the interface and occupy either fcc or hcp sites. The strain induced by the oxygen overlayer causes abrupt changes of the titanium atoms from the hcp to fcc site occupation, creating dislocation lines in the titanium layer, which have the shape of linear trenches. The oxygen atoms above these dislocation lines occupy bridging sites instead of hollow sites and form the zigzag lines. In contrast to the model from Barcaro et al.⁴ oxygen atoms at the elbows of the zigzag lines in the oxygen terminating layer in Jennison's model²⁴ are replaced by titanium atoms. In our measurements the bendings are, in contrast to $\text{TiO}_x/\text{Pt}(111)$, all V-shaped.

Generally, the assignment of the contrast in STM images is always problematic without theoretical simulations. Due to the theoretically supported and widely accepted depiction of titanium empty states as bright protrusions at positive bias voltages on the $r\text{-TiO}_2(110)$ surface,²⁵ we expect this also for the oxidized Pt_3Ti alloy surface. However, it cannot be completely excluded that the alloy bond formation in our case has an influence on the contrast behavior. Since LEED patterns would not distinguish between both discussed models having the same unit cell, our STM images showing only V-

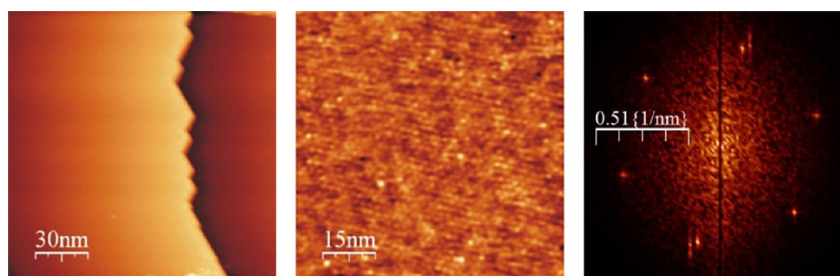


Figure 4. STM images of the $(7 \times 7)\text{R}21.8^\circ$ phase (w' -phase): (a) $150 \times 150 \text{ nm}^2$, $U_B = 1.06 \text{ V}$, $U = 55 \text{ pA}$; (b) $75 \times 75 \text{ nm}^2$, $U_B = -1.08 \text{ V}$, $I = 55 \text{ pA}$; (c) fast Fourier transformation (FFT) from the middle image.

shaped zigzag lines are in agreement with the model of Jennison et al.²⁴ The evolution of defects in the troughs was also seen in TiO_x films on $\text{Pt}(111)$ films.² They were theoretically explained as sites in the troughs, where the bare Pt substrate is exposed due to the absence of titanium atoms.

3.3. w' -Phase. The LEED pattern for the w' -phase indicates a commensurate $(7 \times 7)\text{R}21.8^\circ$ superstructure yielding a hexagonal unit cell of $19.3 \text{ \AA} \times 19.3 \text{ \AA}$ size. It is also described by the matrix

$$\begin{bmatrix} 8 & 3 \\ -3 & 5 \end{bmatrix}$$

STM images obtained at different scales are presented in Figure 4. The film is again very flat and homogeneous and wets the entire surface. Line scans reveal typical single step heights of $\text{Pt}_3\text{Ti}(111)$ indicating a homogeneous thickness of the film across the entire surface. The step edges in Figure 4a partly show a zigzag shape with angles of 120° reflecting the hexagonal symmetry of the oxide overlayer. STM images at higher resolution (Figure 4b) reveal a hexagonal arrangement of bright spots. The Fourier transformation (Figure 4c) confirms the hexagonal symmetry and yields a unit cell size of $19.2 \text{ \AA} \times 19.2 \text{ \AA}$ and is, thus, in good agreement with the LEED results. The HREELS spectrum was shown to be identical to that of the z' -phase with a single loss peak at 525 cm^{-1} , indicating again a single bilayer of TiO stoichiometry.²¹

In the literature similar phases of a variety of systems have been labeled as wagon-wheel-like structures. The name was coined in a publication by Zhang et al.²⁶ on $\text{Cr}/\text{Pt}(111)$ overlayers referring to the shape of the superstructure that resembles the hub and spokes of a wagon-wheel. Quite commonly, long-range superstructures are explained using a Moiré-type model, which arises from long-range coincidence of the metal substrate and the oxide lattice (e.g., $\text{Al}_2\text{O}_3/\text{Ni}_3\text{Al}(111)$).¹¹ Positions, where overlayer atoms are in or close to atop or bridging substrate positions, are imaged brighter than positions where the overlayer atoms are placed in substrate hollow sites.¹¹

$(7 \times 7)\text{R}21.8^\circ$ superstructures with wagon-wheel-like appearance have been reported for $\text{VO}_x/\text{Rh}(111)$ ⁹ and for $\text{TiO}_x/\text{Pt}(111)$.³ Atomically resolved images of these two systems show a hexagonal layer of either vanadium or titanium atoms with a superimposed wagon-wheel-type Moiré pattern. In the case of vanadium the overlayer consists of an oxygen-terminated VO bilayer. The Moiré pattern observed on $\text{VO}_x/\text{Rh}(111)$ can be derived by assuming a lattice vector of 3.1 \AA for the oxide and a rotation of 3.5° with respect to the substrate unit vector.⁹ HREEL spectra for this phase⁹ consist of a single loss peak at 498 cm^{-1} and thus correspond well to the w' -phase on $\text{Pt}_3\text{Ti}(111)$.²¹ For $\text{TiO}_x/\text{Pt}(111)$ similar LEED patterns and

STM images were found and explained by the following structure model: the film consists of a hexagonal bilayer with TiO stoichiometry and a unit cell of $3.18 \text{ \AA} \times 3.18 \text{ \AA}$ size rotated by 3.5° .³ Figure 5 shows the simulation of such a

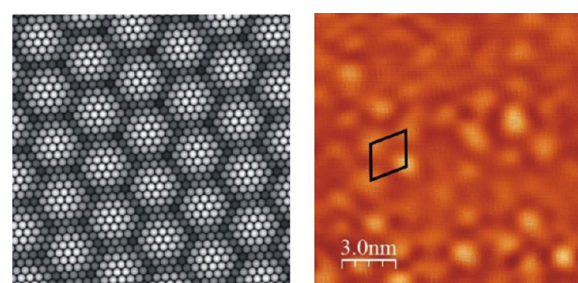


Figure 5. (a) Simulation of a Moiré pattern²⁷ with $a_{\text{substrate}} = 2.76 \text{ \AA}$, $a_{\text{oxide}} = 3.18 \text{ \AA}$, and $\alpha = 3.5^\circ$ together with (b) STM image of the $(7 \times 7)\text{R}21.8^\circ$ phase (w' -phase) ($15 \times 15 \text{ nm}^2$, $U_B = 0.985 \text{ V}$, $I = 52 \text{ pA}$).

surface²⁷ in comparison to a high-resolution STM image of our hexagonal TiO_x -phase on $\text{Pt}_3\text{Ti}(111)$. The agreement is quite good and supports the conclusion that our STM image shows a Moiré pattern arising from a superposition of substrate and oxide lattice.

The w' -phase seems to be the most stable oxide phase on $\text{Pt}_3\text{Ti}(111)$ because it is accessible in both a wide temperature and oxygen dosage range. The thermodynamic stability of this phase may be a result of its hexagonal symmetry that matches the substrate symmetry. The high-resolution image in Figure 4b also shows some point defects in the form of small black holes. Furthermore, a slight modulation of the brightness of the spots is visible. The point defects can most likely be explained by either missing or lower oxidation state titanium atoms. The origin of the brightness modulation could be a partial hydroxylation of the titanium atoms. However, up to now we do not have experimental evidence for this assumption.

3.4. Rect-Phase. This phase is obtained on the $\text{Pt}_3\text{Ti}(111)$ surface after very high oxygen doses (more than 4500 L) at $T = 800 \text{ K}$. The LEED pattern shows an incommensurate overlayer, which corresponds to a

$$\begin{bmatrix} 1.16 & 0.28 \\ 0.58 & 1.56 \end{bmatrix}$$

superstructure with a rectangular unit cell of $3.8 \text{ \AA} \times 3.0 \text{ \AA}$. According to the LEED pattern the unit cell is rotated by $\sim 8^\circ$ with respect to the (1×1) structure of the substrate. The STM images in Figure 6a and b show a flat film that covers the whole surface but leaves open several more or less rectangular spaces of a size between 20 and 400 nm^2 . Most likely, the lattice

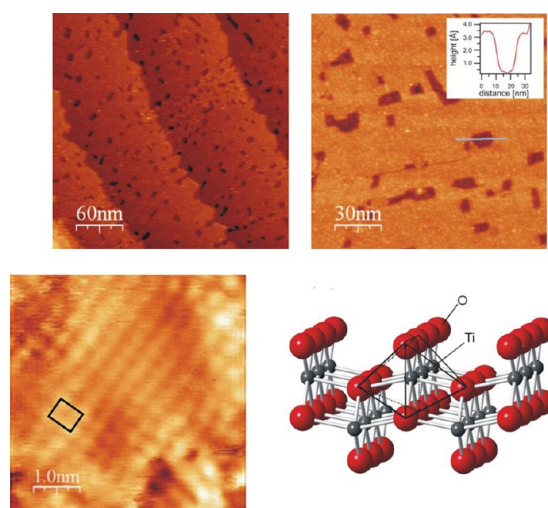


Figure 6. STM images of the rect-TiO₂ phase: (a) 300 × 300 nm², $U_B = 0.87$ V, $I = 60$ pA; (b) 150 × 150 nm², $U_B = 1.09$ V, $I = 65$ pA. The inset shows the depth of the rectangular open spaces, which is about 3 Å. (c) 5 × 5 nm², $U_B = 0.8$ V, $I = 63$ pA. (d) Structure model for this phase adopted from rect-TiO₂/Pt(111)⁵ and rect-VO₂/Pd(111).⁸

mismatch between the oxide film and alloy substrate causes strain within the film, which is released by the formation of these approximately 3 Å deep open spaces (see inset of Figure 6b). The high-resolution image (Figure 6c) shows the arrangement of the atoms with a rectangular unit cell with 3.8 Å × 3.0 Å size close to that found by LEED. As the image is obtained at a small positive bias voltage, probably the empty states of titanium atoms are imaged.

An identical oxide phase was found on Pt(111)^{2,5} consisting of rectangular islands of approximately 2.5 Å height. XPS data revealed a TiO₂ stoichiometry. A similar phase was also reported for rect-VO₂ on Pd(111),⁷ which exhibits a LEED pattern identical to that found for TiO₂ on both discussed surfaces, our Pt₃Ti(111) substrate, and on Pt(111). With the support of DFT calculations a structure model for VO₂ on Pd(111) was developed based on a layer parallel to the cleavage plane of rock salt like VO with two added layers of oxygen.⁸ The resulting rectangular VO₂ layer is oxygen terminated on both sides, and the vanadium atoms of the central plane maintain an octahedral coordination. The resultant triple layer of rect-VO₂ has a height of 4.2 Å and lattice parameters close to the experimental values.⁸ This structure model was adopted by Zhang et al.⁵ to explain the rect-TiO₂ phase, who also pointed out that the structure is already known as lepidocrocite, a γ -FeO(OH) mineral structure. DFT calculations⁵ show a strong

lattice mismatch resulting in strain within the film, which in the case of Pt(111) is released by island growth. On our Pt₃Ti(111) surface such a strain release may be realized by the formation of holes. The different behavior is obviously caused by the different growth processes. While the TiO₂ deposition on Pt(111) using electron beam evaporation results in the formation of single oxide islands,² the direct oxidation of the Pt₃Ti(111) surface forms a continuous oxide film, which can only reduce the upcoming strain by hole formation. Simulated STM images of the rect-phase on Pt(111) with positive bias reveal that the empty Ti states are imaged as bright protrusions, while the oxygen atoms appear dark.⁵ A striking feature is the fact that the interface is formed by an oxygen layer. In the thermodynamically most stable geometry the oxygen atoms prefer atop or bridge positions on the Pt(111) surface rather than the occupation of hollow sites resulting in the observed rotation ($\sim 8^\circ$ in LEED) with respect to the substrate lattice. The interface near the oxygen layer interacts only weakly with the Pt(111) substrate, which might be the reason that the films undergo a phase transition on this substrate upon further annealing. In turn, as the Pt₃Ti(111) surface contains 25% of titanium, and provided that the alloy composition remains unchanged at the high temperature during the oxidation process, the interaction between this alloy surface and the rect-phase should be stronger than on Pt(111), eventually resulting in another rotation angle or in the relaxation of the oxide structure. However, apparently, this is not the case, as both LEED and STM measurements yield the same lattice parameters as found on Pt(111). The phase is also metastable and transforms into the w'-structure upon further annealing. According to the presented model the rect-phase is the only phase on Pt₃Ti(111), which consists of an O–Ti–O triple layer instead of a bilayer.

3.5. z-Phase. The incommensurate z-phase is the phase which is most difficult to obtain, as it exists only in a narrow temperature regime between 800 and 900 K. If the temperature is only slightly higher or the annealing process slightly longer than 10 min a phase transition from the z-phase to the w'-phase is observed. The LEED image shows an incommensurate superstructure, which is represented by the matrix

$$\begin{bmatrix} 2.5 & 0 \\ 1.8 & 3.6 \end{bmatrix}$$

with a rectangular unit cell of 6.8 Å × 8.6 Å and three rotational domains induced by the substrate symmetry. The STM images in Figure 7a–c show a rather rough surface morphology. Although in all cases the same LEED pattern was visible, we

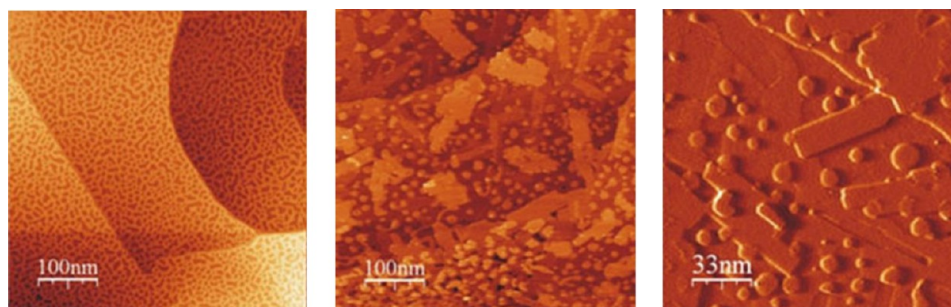


Figure 7. STM images of the z-phase after 900 L of O₂ exposure: (a) 500 × 500 nm², $U_B = 0.6$ V, $I = 50$ pA; and after 2700 L of O₂ exposure: (b) 500 × 500 nm², $U_B = 0.83$ V, $I = 50$ pA; (c) 167 × 167 nm², $U_B = 0.44$ V, $I = 55$ pA.

observed a significant influence of the oxygen dosage on the surface morphology in the STM images.

At rather low dosages of around 900 L the morphology shown in Figure 7a was obtained. A film with a very high number of holes has formed, most likely a consequence of strain release. Line scans show that the holes have an apparent depth of 2.5–3.0 Å. Using higher oxygen dosages of around 2700 L leads to the formation of small islands, which are partly round and partly rectangular with diameters between a few nanometers and nearly a hundred nanometers (see Figure 7b and c). Most of the islands are small and randomly distributed across the surface. All islands have an apparent height of approximately 3 Å. Unfortunately, we were not able to get atomic resolution of these structures with our setup.

A phase with a similar LEED image was also found on $\text{TiO}_x/\text{Pt}(111)$. On this surface the oxide film wets the entire surface as a homogeneous film and exhibits a zigzag structure very similar to that described for the z' -phase.² However, it is not clear why there is such a big difference between the z -phase on $\text{Pt}(111)$ and on $\text{Pt}_3\text{Ti}(111)$. Apparently, the formation of this phase is thermodynamically not favored on the alloy crystal surface.

3.6. Discussion of Preparation Routes. As shown in the previous sections there are striking similarities between the z' -, w' -, and rect-TiO_x phases grown either by direct oxidation of $\text{Pt}_3\text{Ti}(111)$ or by reactive deposition of Ti on $\text{Pt}(111)$.^{2–6} However, there are also some characteristic differences visible which make it worthwhile to compare the two preparation routes. Only the z -phases formed on both substrates seem to show significant differences, the origin of which however is unclear up to now.

The most important difference between the z' -, w' -, and rect -phases grown on either substrate is probably that it was not possible to obtain TiO_x films on $\text{Pt}(111)$ which covered the whole substrate surface completely,² and there were always some uncovered $\text{Pt}(111)$ patches visible. For the phases obtained by direct oxygen exposure of $\text{Pt}_3\text{Ti}(111)$ this was definitely never the case, even for the oxygen-poor z' - TiO_x phase.

Also worth mentioning is the fact that independent from the Ti deposition conditions on $\text{Pt}(111)$ the formation of additional disordered oxide clusters was observed (see Figure 8). These clusters appear either as 3D islands on the formed TiO_x patches or as 2D wormlike structures on the uncovered Pt areas.² In both cases X-ray photoelectron diffraction (XPD)

measurements showed indications for fully oxidized Ti in the TiO_2 rutile modification.²⁸ The appearance of the TiO_2 clusters has been explained by local or overall excess of Ti during the deposition process. The clusters have been proposed to act as growth precursors for the ordered TiO_x phases. Higher temperatures and higher oxygen pressures amplify the cluster growth, which indicates a competition between the thermodynamically favored TiO_2 clusters and the ordered 2D-suboxide phases. Obviously, the completely different oxidation process on the Pt_3Ti alloy surface hinders effectively the formation of such clusters. In this case the rate of Ti segregation from the bulk limits the Ti amount on the surface resulting in very homogeneous and long-range ordered TiO_x films.

4. CONCLUSIONS

Four different atomically thin oxide phases were prepared on $\text{Pt}_3\text{Ti}(111)$ depending on substrate temperature, oxygen pressure, and oxygen exposure. All phases were characterized by LEED and STM. Two commensurate phases were found, which both form very homogeneous films that cover the entire surface. The films consist in both cases of a Ti–O bilayer with oxygen termination. The z' -phase possesses a rectangular unit cell and consists of stripes of denser packed titanium atoms separated by troughs. The stripes exhibit a zigzag motif, which is formed by titanium atoms with a higher (4-fold) oxygen coordination as well as titanium atoms which are only 3-fold coordinated. The w' -phase consists of a hexagonal Ti–O layer with a lattice parameter of $a = 3.19$ Å, which is rotated by 3.5° with respect to the densely packed substrate atom rows. STM reveals a long-range hexagonal Moiré pattern with a unit cell size of 19.3 Å \times 19.3 Å, which reflects the coincidence points between the oxide film and substrate lattice. Both phases are stable against thermal annealing.

After very high oxygen dosages an incommensurate rect-TiO_2 -phase was found, in which the titanium atoms are higher oxidized than in the two commensurate oxide phases. Its structure can be derived from the lepidocrocite structure. It is made of an O–Ti–O triple layer with octahedrally coordinated titanium atoms between two oxygen layers. It forms a continuous film that contains several rectangular open spaces, apparently to release strain induced by the lattice mismatch between substrate and oxide. This phase is unstable against further thermal annealing and undergoes a phase transition toward the w' -phase. The second incommensurate phase is only accessible at high oxygen pressures in a very small temperature range. Its surface morphology is very disordered either consisting of a film with a large number of holes or a variety of small round and rectangular islands. It is also very unstable against thermal annealing.

The titanium oxide phases grown on $\text{Pt}_3\text{Ti}(111)$ are in many aspects similar to phases prepared by reactive deposition of titanium on $\text{Pt}(111)$ by Sedona et al.² They all show identical LEED patterns as well as in most cases also a very similar appearance in atomically resolved STM images. Major differences can be found only in the macroscopic morphology. While the commensurate z' - and w' -phases on $\text{Pt}_3\text{Ti}(111)$ always cover the whole surface completely, this was not observed on $\text{TiO}_x/\text{Pt}(111)$. Moreover, we never had any indication of fully oxidized TiO_2 clusters on the surface, which, by contrast, had been found by Sedona et al. on all titanium oxide phases on $\text{Pt}(111)$, probably as a consequence of the different, i.e., reactive, deposition process.² It can thus be stated that a lower reaction rate with Ti atoms distributed

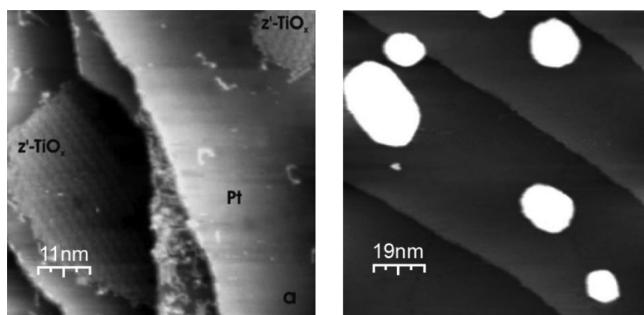


Figure 8. STM images of corresponding TiO_x phases formed with reactive Ti deposition on $\text{Pt}(111)$ reproduced from Sedona et al.:² (a) z' - TiO_x phase with wormlike structures on the bare Pt patches (60×60 nm²; $U_B = 0.8$ V, $I = 0.8$ nA) and (b) w' - TiO_x phase with 3D clusters on the top (110×110 nm²; $U_B = 1.0$ V, $I = 1.2$ nA).

homogeneously across the whole alloy surface results in a more controlled oxide growth.

The Pt₃Ti(111) crystal proved to be a well-suited template for the growth of highly ordered ultrathin titanium oxide films, which are easily reproducible. Especially the z'-, w'-, and, with some limitations, the rect-TiO₂ phase are excellent surfaces for further surface science studies on titanium oxide like, e.g., cluster growth, surface chemistry, or defect chemistry.

AUTHOR INFORMATION

Corresponding Author

*Tel.: +492461615881. E-mail: m.moors@fz-juelich.de.

Notes

The authors declare no competing financial interest.

ACKNOWLEDGMENTS

We kindly acknowledge financial support from the Deutsche Forschungsgemeinschaft (DFG) through SFB 624 Templates.

REFERENCES

- Boffa, A. B.; Galloway, H. C.; Jacobs, P. W.; Benitez, J. J.; Batteas, J. D.; Salmeron, M.; Bell, A. T.; Somorjai, G. A. The Growth and Structure of Titanium-Oxide Films on Pt(111) Investigated by LEED, XPS, ISS, and STM. *Surf. Sci.* **1995**, *326* (1–2), 80–92.
- Sedona, F.; Rizzi, G. A.; Agnoli, S.; Xamena, F. X. L. I.; Papageorgiou, A.; Ostermann, D.; Samb, M.; Finetti, P.; Schierbaum, K.; Granozzi, G. Ultrathin TiO_x films on Pt(111): A LEED, XPS, and STM investigation. *J. Phys. Chem. B* **2005**, *109* (51), 24411–24426.
- Sedona, F.; Agnoli, S.; Granozzi, G. Ultrathin wagon-wheel-like TiO_x phases on Pt(111): A combined low-energy electron diffraction and scanning tunneling microscopy investigation. *J. Phys. Chem. B* **2006**, *110* (31), 15359–15367.
- Barcaro, G.; Sedona, F.; Fortunelli, A.; Granozzi, G. Structure of a TiO_x zigzag-like monolayer on Pt(111). *J. Phys. Chem. C* **2007**, *111* (16), 6095–6102.
- Zhang, Y.; Giordano, L.; Pacchioni, G.; Vittadini, A.; Sedona, F.; Finetti, P.; Granozzi, G. The structure of a stoichiometric TiO₂ nanophase on Pt(111). *Surf. Sci.* **2007**, *601* (16), 3488–3496.
- Sedona, F.; Granozzi, G.; Barcaro, G.; Fortunelli, A. Defect evolution in oxide nanophases: The case of a zigzag-like TiO_x phase on Pt(111). *Phys. Rev. B* **2008**, *77* (11), 115417.
- Surnev, S.; Kresse, G.; Sock, M.; Ramsey, M. G.; Netzer, F. P. Surface structures of ultrathin vanadium oxide films on Pd(111). *Surf. Sci.* **2001**, *495*, 91–106.
- Kresse, G.; Surnev, S.; Ramsey, M. G.; Netzer, F. P. First-principles calculations for V_xO_y grown on Pd(111). *Surf. Sci.* **2001**, *492* (3), 329–344.
- Schoiswohl, J.; Surnev, S.; Sock, M.; Eck, S.; Ramsey, M. G.; Netzer, F. P.; Kresse, G. Reduction of vanadium-oxide monolayer structures. *Phys. Rev. B* **2005**, *71* (16), 165437.
- Surnev, S.; Sock, M.; Kresse, G.; Andersen, J. N.; Ramsey, M. G.; Netzer, F. P. Unusual CO adsorption sites on vanadium oxide-Pd(111) "inverse model catalyst" surfaces. *J. Phys. Chem. B* **2003**, *107* (20), 4777–4785.
- Degen, S.; Krupski, A.; Kralj, M.; Langner, A.; Becker, C.; Sokolowski, M.; Wandelt, K. Determination of the coincidence lattice of an ultra thin Al₂O₃ film on Ni₃Al(111). *Surf. Sci.* **2005**, *576* (1–3), L57–L64.
- Hamm, G.; Barth, C.; Becker, C.; Wandelt, K.; Henry, C. R. Surface structure of an ultrathin alumina film on Ni₃Al(111): A dynamic scanning force microscopy study. *Phys. Rev. Lett.* **2006**, *97* (12), 126106.
- Gritschneider, S.; Becker, C.; Wandelt, K.; Reichling, M. Disorder or complexity? Understanding a nanoscale template structure on alumina. *J. Am. Chem. Soc.* **2007**, *129* (16), 4925–4928.
- Schmid, M.; Kresse, G.; Buchsbaum, A.; Napetschnig, E.; Gritschneider, S.; Reichling, M.; Varga, P. Nanotemplate with holes: Ultrathin alumina on Ni₃Al(111). *Phys. Rev. Lett.* **2007**, *99* (19), 196104.
- Bardi, U.; Ross, P. N. Superlattice Leed Patterns Observed from [111] and [100] Oriented Single-Crystals of TiPt₃. *Surf. Sci.* **1984**, *146* (1), L555–L560.
- Bardi, U.; Dahlgren, D.; Ross, P. N. Structure and Chemisorptive Properties of the Pt₃Ti Surface. *J. Catal.* **1986**, *100* (1), 196–209.
- Chen, W.; Paul, J. A. K.; Barbieri, A.; Hove, M. A. V.; Cameron, S.; Dwyer, D. J. Structure determination of Pt₃Ti(111) by automated tensor LEED. *J. Phys.: Condens. Matter* **1993**, *5* (27), 4585.
- Chen, W. H.; Severin, L.; Goethelid, M.; Hammar, M.; Cameron, S.; Paul, J. Electronic and Geometric Structure of Clean Pt₃Ti(111). *Phys. Rev. B* **1994**, *50* (8), 5620–5627.
- Chen, W.; Cameron, S.; Goethelid, M.; Hammar, M.; Paul, J. Redox Properties of Titanium Oxides on Pt₃Ti. *J. Phys. Chem.* **1995**, *99* (34), 12892–12895.
- Chen, W. H.; Chulkov, E.; Paul, J. Band structure calculations of Pt and Pt₃Ti. *Phys. Scr.* **1996**, *54* (4), 392–396.
- Le Moal, S.; Moors, M.; Essen, J. M.; Breinlich, C.; Becker, C.; Wandelt, K. Structural and compositional characterization of ultrathin titanium oxide films grown on Pt₃Ti(111). *J. Phys.: Condens. Matter* **2013**, *25* (4), 045013.
- Degen, S. Aufbau eines Tieftemperaturrastertunnelmikroskops und Messungen auf i₃Al (111). *Ph.D. Thesis*, University of Bonn, January 2006.
- Barcaro, G.; Agnoli, S.; Sedona, F.; Rizzi, G. A.; Fortunelli, A.; Granozzi, G. Structure of Reduced Ultrathin TiO_x Polar Films on Pt(111). *J. Phys. Chem. C* **2009**, *113* (14), 5721–5729.
- Jennison, D. R.; Dulub, O.; Hebenstreit, W.; Diebold, U. Structure of an ultrathin TiO_x film, formed by the strong metal support interaction (SMSI), on Pt nanocrystals on TiO₂(110). *Surf. Sci.* **2001**, *492* (1–2), L677–L687.
- Diebold, U. The surface science of titanium dioxide. *Surf. Sci. Rep.* **2003**, *48* (5–8), 53–229.
- Zhang, L. P.; van Ek, J.; Diebold, U. Spatial self-organization of a nanoscale structure on the Pt(111) surface. *Phys. Rev. B* **1999**, *59* (8), 5837–5846.
- Simulation software of Ph.D. thesis of A. Spänig. University of Bonn, 2004.
- Sedona, F.; Eusebio, M.; Rizzi, G. A.; Granozzi, G.; Ostermann, D.; Schierbaum, K. Epitaxial TiO₂ nanoparticles on Pt(111): a structural study by photoelectron diffraction and scanning tunneling microscopy. *Phys. Chem. Chem. Phys.* **2005**, *7* (4), 697–702.